Supporting Information

Surface doping of cobalt nanoparticles by selenium anion to steer the selectivity in electrocatalytic nitrate reduction

Xuan Zheng[a], Shifei Ding[a], Mingyue Zhu[a], Fengjun Ma[a], Jiace Hao[a], Shuanglong Lu[a], Fang Duan[a], Han Zhu*[a], Chenglong Wang*[c], and Mingliang Du*[a]

a. Key Laboratory of Synthetic and Biological Colloids, Ministry of Education, School of Chemical and Material Engineering, Jiangnan University, Wuxi, Jiangsu 214122, P. R. China. E-mail: zhysw@jiangnan.edu.cn; du@jiangnan.edu.cn

b. Engineering Research Center for Eco-Dyeing and Finishing of Textiles, Ministry of Education, Zhejiang Sci-Tech University, Hangzhou 310018, P. R. China. E-mail: wcl_charles@126.com

Determination of ammonia (NH_3)

The concentration of ammonia product was spectrophotometrically detected by the standard indophenol blue indicator method. Briefly, 2 mL of the solution product, 2 mL of a 1 M NaOH solution with 5% salicylic acid and 5% sodium citrate, 1 mL of 0.05 M NaClO and 0.2 mL of 1% sodium nitroferricyanide (III) dihydrate ($C_5FeN_6Na_2O{\cdot}2H_2O$) solution were mixed. After standing in the dark for 2 h, the concentration of indophenol blue was detected by ultraviolet-visible (UV-Vis) spectrophotometer at a wavelength of 650 nm in the absorption spectrum. For the quantitative determination of the amount of NH_4^+, a standard NH_4Cl solution was used to calibrate the concentration-absorbance standard curve for a series of concentrations (Fig. S1).

Determination of nitrite (NO_2^-)

Firstly, 0.2 g of N-(1-naphthyl) ethylenediamine dihydrochloride, 4 g of p-aminobenzenesulfonamide, and 10 mL of phosphoric acid (ρ = 1.685 g mL^{-1}) were added into 50 mL of deionized water and mixed thoroughly as the color reagent. When testing the electrolyte from electrolytic cell, it should be diluted to the detection range. Then 2 mL of the diluted electrolyte and 40 μL of color reagent were mixed together. After 20 min at room temperature, the absorption spectrum was measured by using a UV–vis spectrophotometer (UV2600), and the absorption intensity was recorded at a wavelength of 540 nm. A series of standard potassium nitrite solutions were used to obtain the concentration–absorbance curve by the same processes. To quantify the amount of NO_2^-, a calibration curve was built using standard KNO_2 solution (Fig. S2).

Determination of hydrazine hydrate (N_2H_4)

Firstly, 300 mL of C_2H_5OH, 30 mL of concentrated HCl, and 5.99 g of $C_9H_{11}NO$ were mixed together to be used as the color reagent. Then, 2 mL of color reagent was added to 2 mL of 0.5 M K_2SO_4 electrolyte before and after 2 h of electrolysis. Next, the solution was stirred under ambient conditions for 30 min. The absorbance curves at 455 nm were measured via the UV-Vis spectrophotometer. To quantify the amount of N_2H_4, a calibration curve was built using standard N_2H_4 solution (Fig. S3).

Calculation of the FE_{NH4+} and $Yield_{NH4+}$

$$Yield_{NH4+}\,(mmol\ h^{-1}\ mg_{cat}^{-1}) = C_{NH4+} \times V / (1000 \times mg_{cat} \times t) \quad (1)$$

$$FE_{NH4+}(\%) = (8 \times F \times C_{NH4+} \times V) / (1000 \times Q) \times 100\% \quad (2)$$

where V is the volume of electrolyte (0.05 L); C_{NH4+} is the concentration of NH_4^+ (μmol L^{-1}); t is the reaction time (2 h); mg_{cat} is mass normalization; F represents the Faraday constant (96485 C mol^{-1}); Q is the electric charge (C).

^{15}N and ^{14}N 1H-NMR measurements

The electrolyte was prepared with $K^{15}NO_3$/ $K^{14}NO_3$ as nitrogen sources. After

electrolysis, 500 μL of electrolyte was extracted and mixed with 150 μL of 0.5 M H_2SO_4 solution to adjust the pH value. Then, 100 μL of D_2O was added, and qualitative analysis was conducted using DMSO (50 μL) as an external standard for ^1H NMR at a frequency of 400 MHz. All NMR measurements were carried out with water suppression and 128 scans for qualitative analysis.

In-situ Raman spectroscopy

In-situ Raman spectroscopy was recorded on the above-mentioned Raman microscope under controlled potentials by electrochemical workstation. The operando electrochemical Raman test was carried out in a round home-made electrolyzer. A platinum wire and Ag/AgCl electrode were served as the counter and reference electrode, respectively. The in-situ Raman measurements were carried out over a range of 100 ~ 4000 cm^{-1} during the chronoamperometry measurements at -0.7 V vs. RHE, and the dwell time at each potential was 5 min.

DFT simulation

Spin-polarized density functional theory (DFT) calculations were carried out via Vienna ab initio simulation package (VASP) utilizing the projector augmented wave (PAW) potentials with a plane wave cutoff energy of 400 eV. The generalized gradient approximation (GGA) functional of Perdew, Burke, and Ernzerhof (PBE) was applied as the exchange-correlation functional. To prevent the interaction between two adjacent layers, a vacuum layer of 15 A were adopt for all the surface model. We employed a gamma-centered k-point grid to sample the Brillouin zones. The convergence criteria of electronic energies were 10^{-5} eV, and the atomic forces of 0.03 eV/A was adopt for all calculations.

To simulate the NO_3RR process on Se@Co/CNFs and Co/CNFs catalysts, a p(3 × 3) supercell slab of Co (111) surface doped with 1 Se atom (Se@Co) and a p(3 × 3) supercell slab of Co (100) surface were chosen as the DFT calculation models. 4×4×1 k-point meshes were used for Se@Co and Co (100) models.

The NO_3RR on different catalysts surfaces were simulated according to the following reactions:

$$HNO_3(l)+8H^+ +8e^-\rightarrow NO3^*+9H^++9e^-$$
$$NO_3^*+9H^++9e^-\rightarrow NO_2OH^*+8H^++8e^-$$
$$NO_2OH^*+8H^++8e^-\rightarrow NO_2^*+H_2O+7H^++7e^-$$
$$NO_2^*+H_2O+7H^++7e^-\rightarrow NOOH^*+H_2O+6H^++6e^-$$
$$NOOH^*+H_2O+6H^++6e^-\rightarrow NO^*+2H_2O+5H^++5e^-$$
$$NO^*+2H_2O+5H^++5e^-\rightarrow NOH^*+2H_2O+4H^++4e^-$$
$$NOH^*+2H_2O+4H^++4e^-\rightarrow N^*+3H_2O+3H^++3e^-$$
$$N^*+3H_2O+3H^++3e^-\rightarrow NH^*+3H_2O+2H^++2e^-$$
$$NH^*+3H_2O+2H^++2e^-\rightarrow NH_2^*+3H_2O+H^++ e^-$$
$$NH_2^*+3H_2O+H^++e^-\rightarrow NH_3^*+3H_2O$$
$$NH_3^*+3H_2O\rightarrow NH_3(g)+3H_2O$$

where the * represent the adsorption site. The Gibbs free energy change (ΔG，298 K) of each step was calculated by the following equation:

$$\Delta G = \Delta E + \Delta EZPE - T\Delta S$$

where ΔE is the adsorption energy, ΔZPE is the zero point energy difference and TΔS

is the entropy difference between the gas phase and adsorbed state.

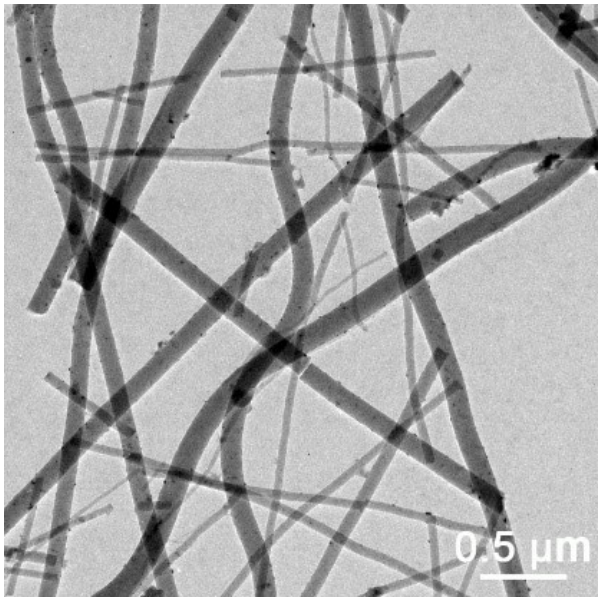

Fig. S1. Low-magnification TEM images of Se@Co/CNFs.

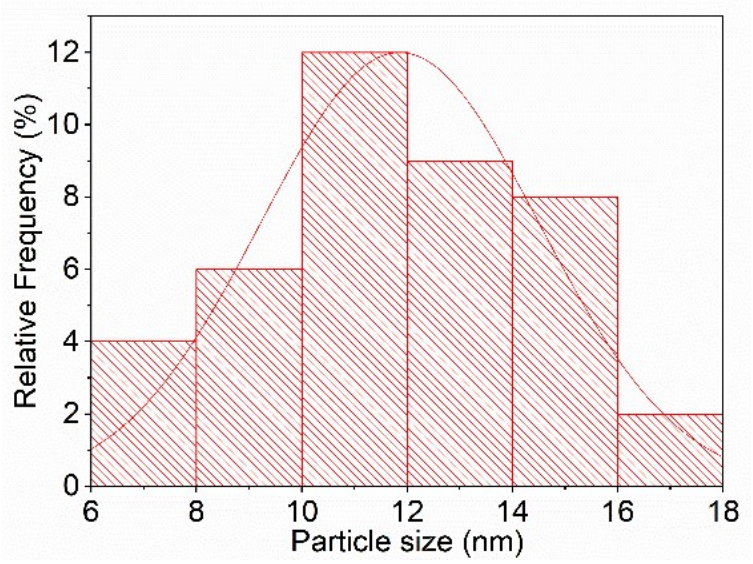

Fig. S2. The size distribution profile of Se@Co NPs immobilized on CNFs.

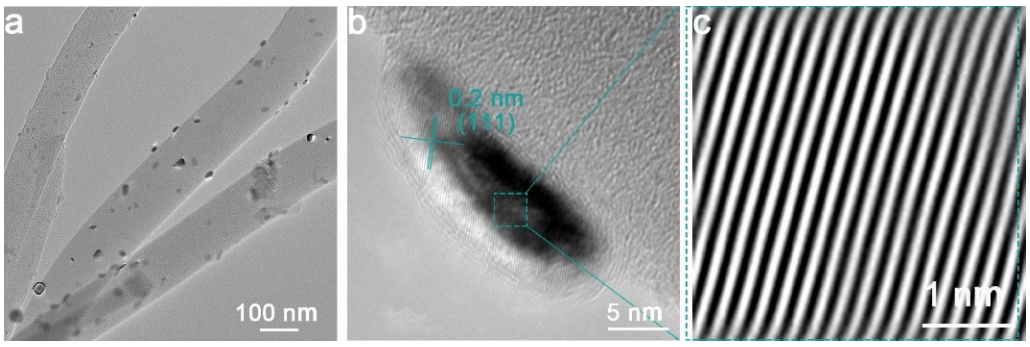

Fig. S3. (a) TEM and (b) HRTEM images of Co/CNFs. (c) IFFT patterns of the (111) plane of Co/CNFs displayed in the HRTEM image.

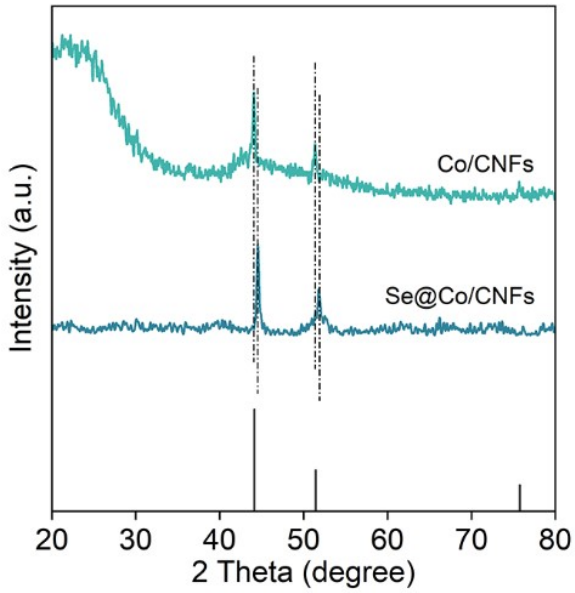

Fig. S4. XRD patterns of Co/CNFs and Se@Co/CNFs.

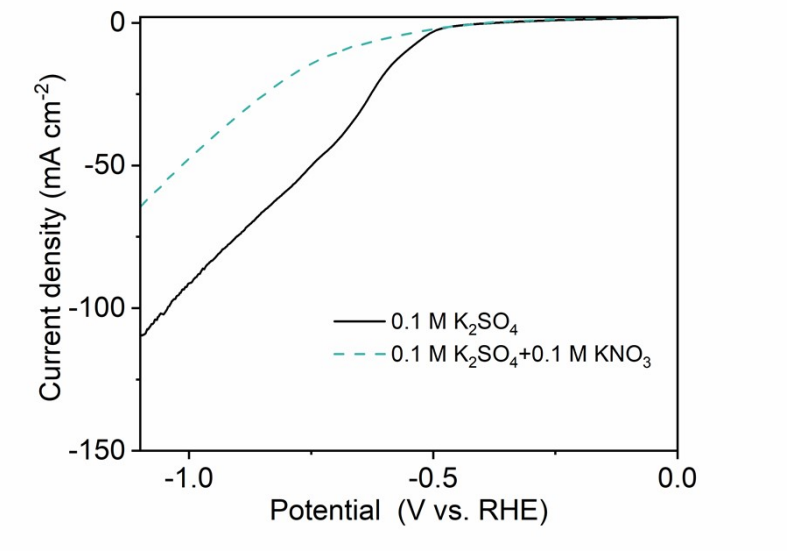

Fig. S5. LSV curves of Co/CNFs in 0.1 M K_2SO_4 with and without 0.1 M KNO_3.

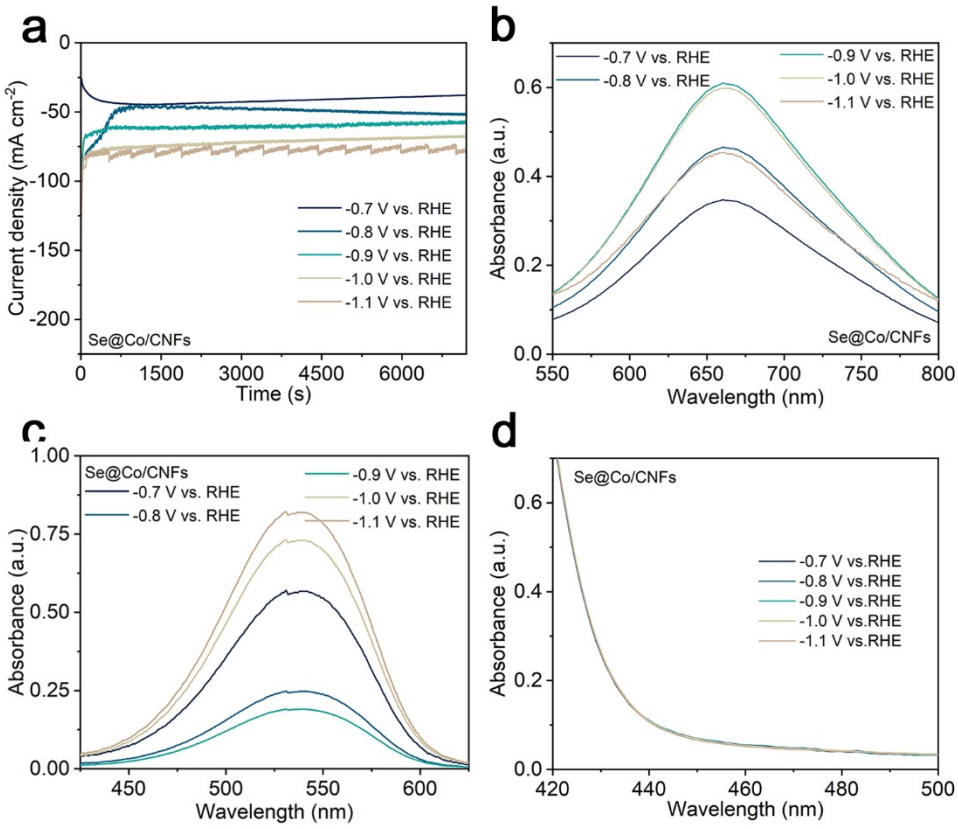

Fig. S6. (a) Chronoamperometry curves of Se@Co/CNFs at various potentials for 2 h in Ar-saturated 0.1 M K_2SO_4 and 0.1 M KNO_3. (b) UV-Vis absorption spectra of NH_4^+ after 2 h electrolysis of Se@Co/CNFs at various potentials (diluted 50 times). (c) UV-Vis absorption spectra of NO_2^- after 2 h electrolysis of Se@Co/CNFs at various potentials (diluted 100 times). (d) UV-Vis absorption spectra of N_2H_4 after 2 h electrolysis of Se@Co/CNFs at various potentials.

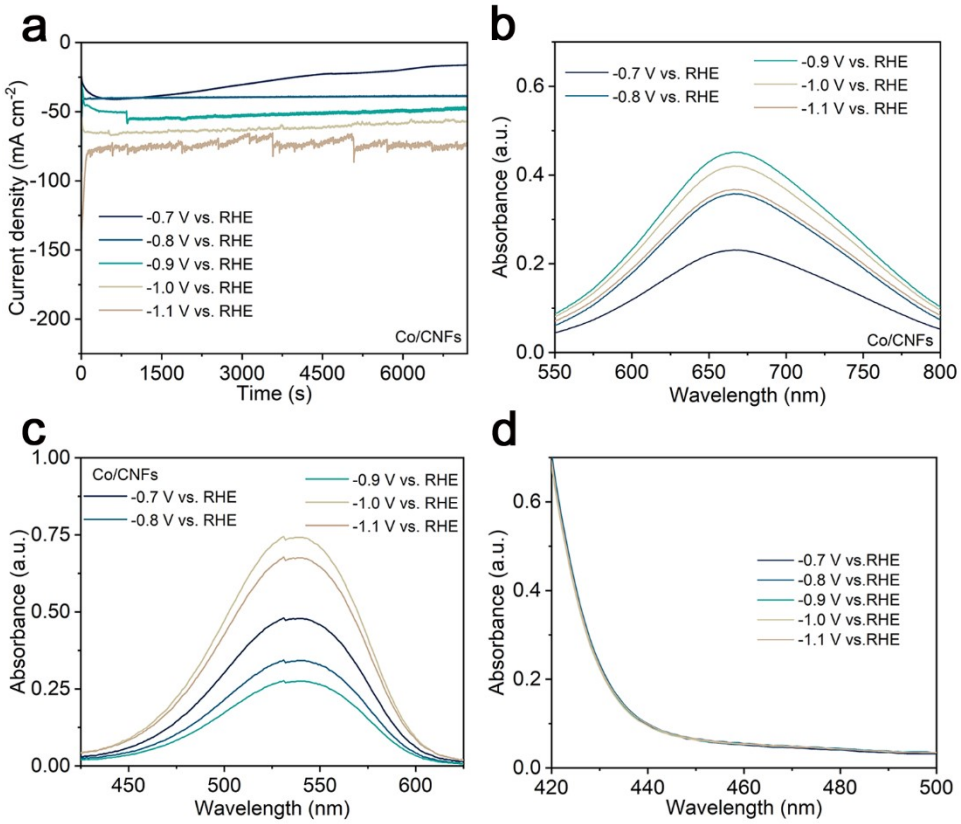

Fig. S7. (a) Chronoamperometry curves of Co/CNFs at various potentials for 2 h in Ar-saturated 0.1 M K_2SO_4 and 0.1 M KNO_3. (b) UV-Vis absorption spectra of NH_4^+ after 2 h electrolysis of Co/CNFs at various potentials (diluted 50 times). (c) UV-Vis absorption spectra of NO_2^- after 2 h electrolysis of Co/CNFs at various potentials (diluted 120 times). (d) UV-Vis absorption spectra of N_2H_4 after 2 h electrolysis of Co/CNFs at various potentials.

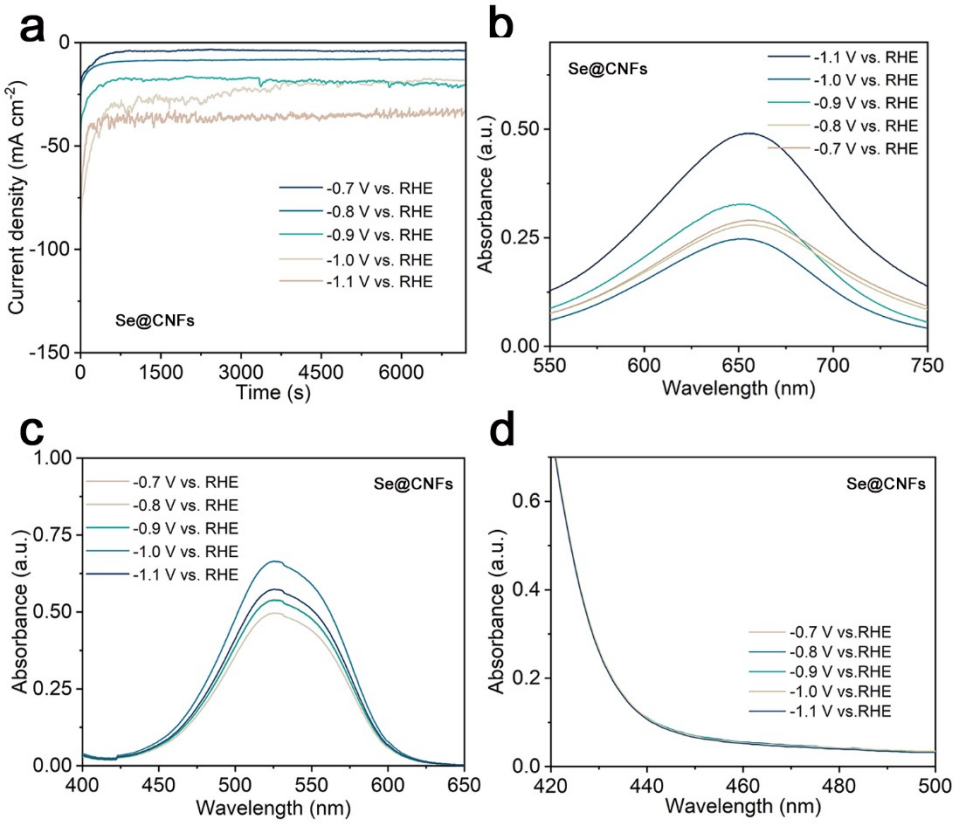

Fig. S8. (a) Chronoamperometry curves of Se@CNFs at various potentials for 2 h in Ar-saturated 0.1 M K_2SO_4 and 0.1 M KNO_3. (b) UV-Vis absorption spectra of NH_4^+ after 2 h electrolysis of Se@CNFs at various potentials (diluted 5 times). (c) UV-Vis absorption spectra of NO_2^- after 2 h electrolysis of Se@CNFs at various potentials (diluted 30 times). (d) UV-Vis absorption spectra of N_2H_4 after 2 h electrolysis of Se@CNFs at various potentials.

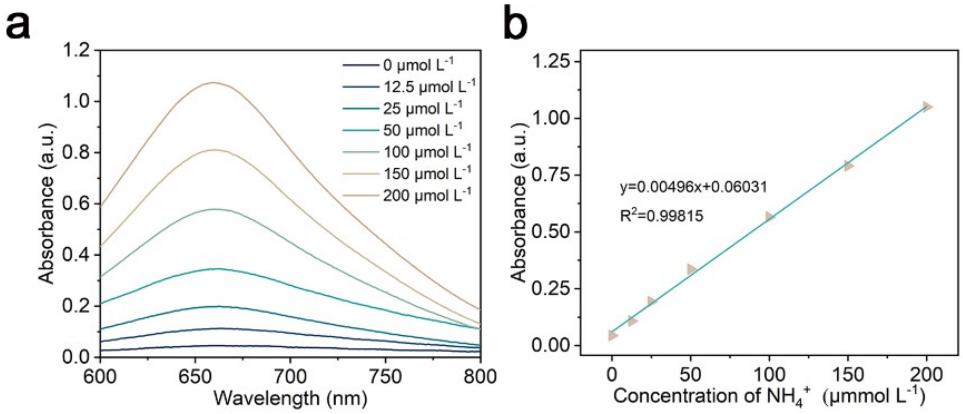

Fig. S9. (a) UV-Vis absorption spectra of indophenol assays with NH_4^+ ions after incubated for 2 h at room temperature. (b) The calibration curve used for estimation of NH_4^+.

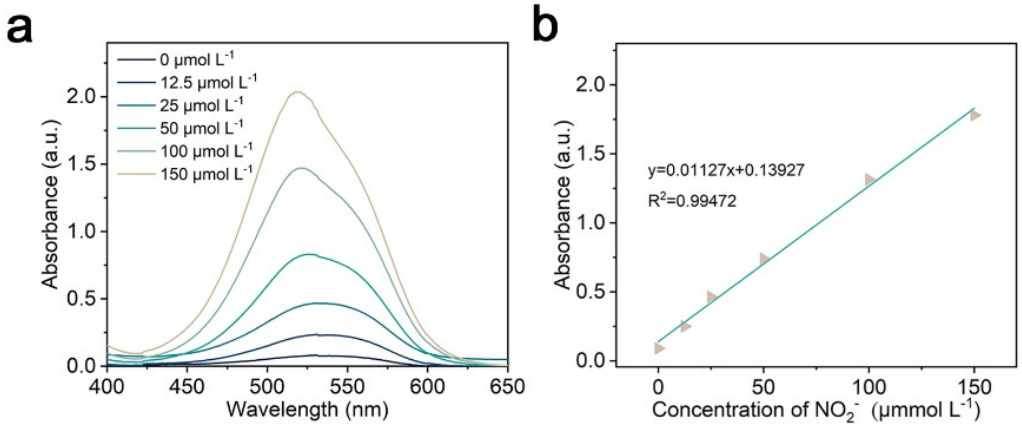

Fig. S10. (a) UV-Vis absorption spectra of various NO_2^- concentrations at room temperature. (b) The calibration curve used for estimation of NO_2^-.

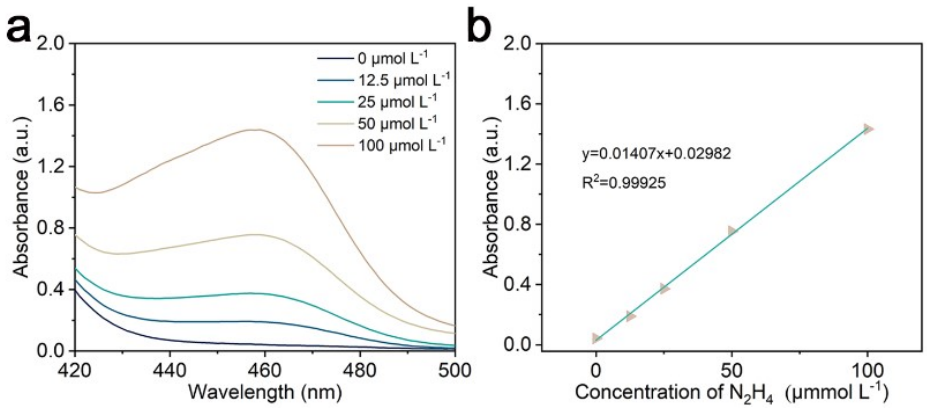

Fig. S11. (a) UV-Vis absorption spectra of various N_2H_4 concentrations at room temperature. (b) The calibration curve used for estimation of N_2H_4.

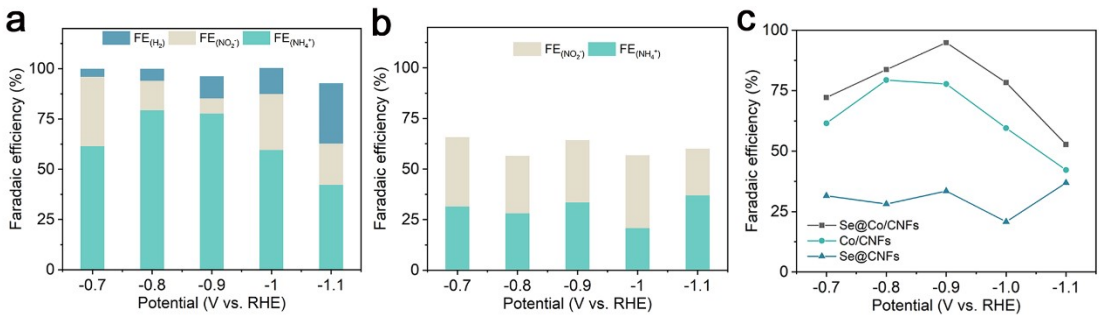

Fig. S12. FEs of different products (NH_4^+, NO_2^- and H_2) for a) Co/CNFs and b) Se@CNFs at different applied potentials from -0.7 to -1.1 V vs. RHE.

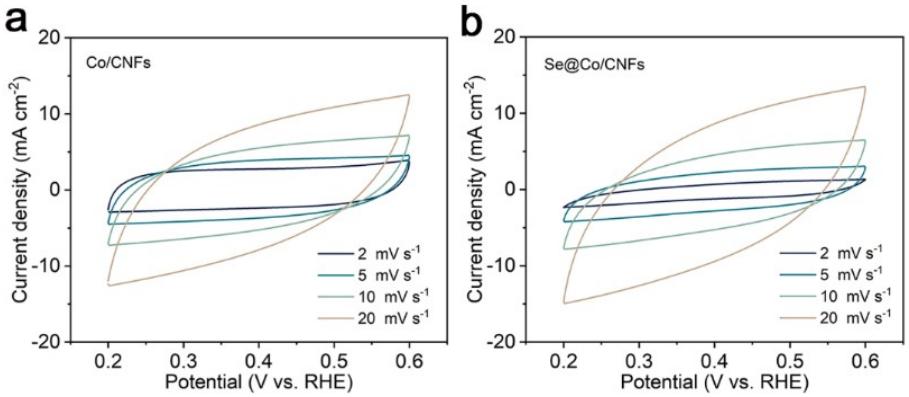

Fig. S13. Cyclic voltammograms of (a) Co/CNFs and (b) Se@Co/CNFs in an Ar saturated 0.1 M KNO_3 and 0.1 M K_2SO_4 electrolyte.

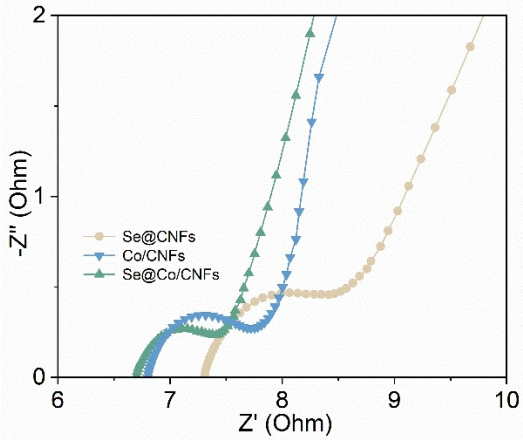

Fig. S14. Electrochemical impedance spectroscopy of Se@CNFs, Co/CNFs and Se@Co/CNFs.

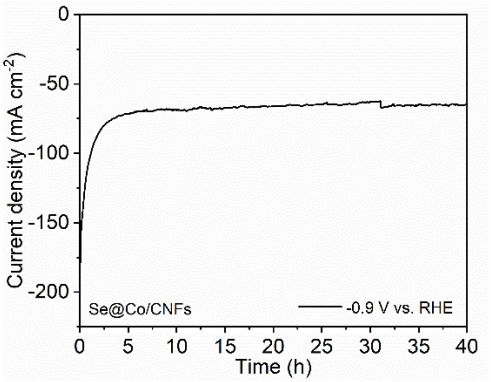

Fig. S15. Electrochemical stability tests of Se@Co/CNFs in an H-cell at a constant potential of -0.9 V vs RHE.

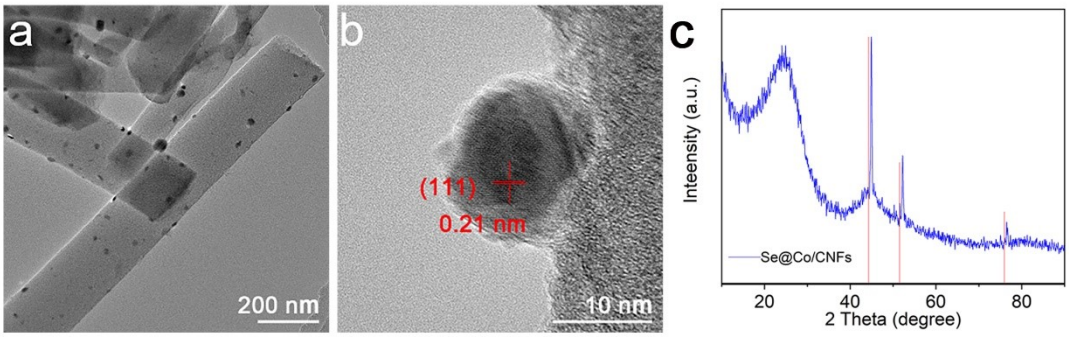

Fig. S16. (a) TEM images, (b) HRTEM images and (c) XRD patterns of Se@Co/CNFs after the stability test.

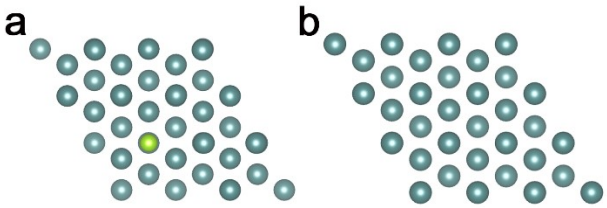

Fig. S17. The DFT relaxed models. The light green and dark green spheres represent Se and Co atoms, respectively.

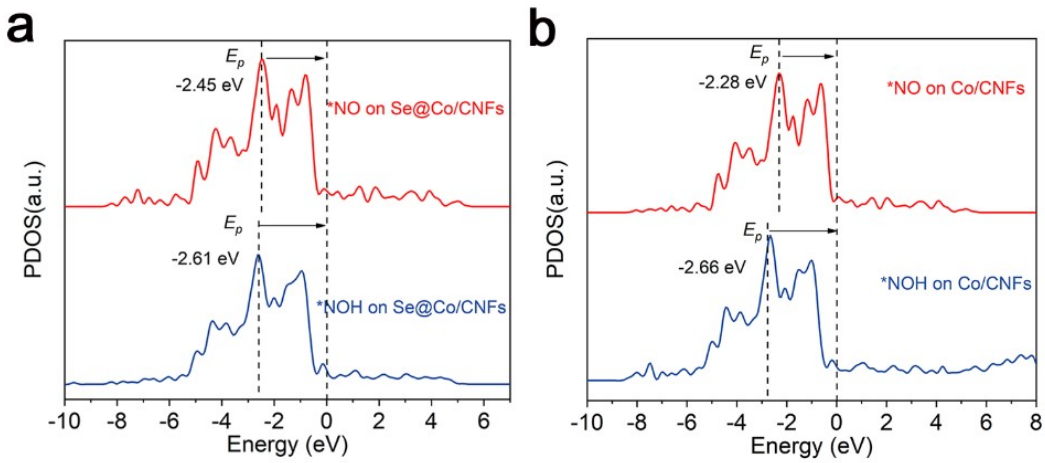

Fig. S18. PDOS profiles of *NO and *NOH intermediates on (a) Se@Co/CNFs and (b) Co/CNFs.

Table S1. Metal content of the Se@Co/CNFs and Co/CNFs determined by ICP-AES.

Elements	Se@Co/CNFs		Co/CNFs
	Co	Se	Co
Atomic-percentage (at. %)	4.12	1.14	4.68

Table S2. Comparison of performance of Se@Co/CNFs with reported catalysts by electrocatalytic nitrate reduction.

Catalysts	**Potential (V vs. RHE)**	**FE(%)**	**Yield rate (mmol h^{-1} mg^{-1})**	**Ref.**
Se@Co/CNFs	-0.9	91.40	3.7	This work
Co@NC-4	-0.8	95.00	1.39	[1]
Cu(B)	-0.8	88.70	0.261	[2]
Co@JDC	-1.0	96.9	2.8	[3]
CoOx nanosheets	-0.3	93.4	4.847	[4]
CoP NAs	-0.7	100%	0.569	[5]
CuNi alloy	-0.22	95.70%	2.55	[6]
Fe_3C	-0.5	96.7%	1.19	[7]
CoP PANSs	-0.5	94.24	1.13	[8]
Cu-Co_3O_4	-0.6	86.51	0.0367	[9]
Cu-SnS_2	-0.7	93.8173	0.63	[10]
Ag/ZnO	-0.6	66	0.516	[11]

References

[1] B. Zhang, F.S Yu, Y. H. Hong, Y. Z. Zhou, Y. H. Wang, S. B. Zhang and L. H. Zhang, Electron-deficient Co Modulated by Constructing Heterojunction Co@NC Boosting Electroreduction of Nitrate to Ammonium, Inorg. Chem. Front., 2024, Accepted Manuscript
[2] L. H. Zhang, Y. T. Jia, J. Y. Zhan, G. M. Liu, G. H. Liu, F. Li and F S. Yu, Dopant-Induced Electronic States Regulation Boosting Electroreduction of Dilute Nitrate to Ammonium, Angew. Chem. Int. Ed. 2023, 62, e202303483.
[3] J. Q. Wang, J. Liang, P. Y. Liu, Z. Yan, L. X. Cui, L. C. Yue, L. C. Zhang, Y. C. Ren, T. S. Li, Y. L. Luo, Q. Liu, X. E. Zhao, N. Li, B. Tang, Y. Liu S. Y. Gao, Abdullah M. Asiri, H. G. Hao, R. Gao and X. P. Sun, Biomass Juncus derived carbon decorated with cobalt nanoparticles enables high-efficiency ammonia electrosynthesis by nitrite reduction, J. Mater. Chem. A, 2022, 10, 2842-2848.
[4] J. Wang, C. Cai, Y. Wang, X. Yang, D. Wu, Y. Zhu, M. Li, M. Gu and M. Shao, Electrocatalytic reduction of nitrate to ammonia on low-cost ultrathin CoOx nanosheets. ACS Catalysis 2021, 11, 15135-15140.
[5] S. Ye, Z. Chen, G. Zhang, W. Chen, C. Peng, X. Yang, L. Zheng, Y. Li, X. Ren, H.Cao, Elucidating the activity, mechanism and application of selective electrosynthesis of ammonia from nitrate on cobalt phosphide, Energy &Environmental Science 2022, 15, 760-770.
[6] Z. J. Zhang, Y. Liu, X. Z. Su, Z. W. Zhao, Z. K. Mo, C. Y. Wang, Y. L. Zhao, Y. Chen, and S. Y. Gao, Electro-triggered Joule heating method to synthesize single-phase CuNi nano-alloy catalyst for efficient electrocatalytic nitrate reduction toward ammonia, 2023, 16(5): 6632-6641.
[7] Y. Y. Wang, L. L. Zhang, Y. J. Niu, D. Fang, J. Wang, Q. X. Su and C. Wang, Boosting NH_3 production from nitrate electroreduction via electronic structure engineering of Fe_3C nanoflakes, Green Chem., 2021, 23, 7594-7608.
[8] Y. Jia, Y. G. Ji, Q. Xue, F. M. Li, G. T. Zhao, P. J. Jin, S. N. Li and Y. Chen, Efficient Nitrate-to-Ammonia Electroreduction at Cobalt Phosphide Nanoshuttles. ACS Appl Mater Interfoces.2021:13:45521-45527.
[9] Z. D. Niu, S. Y. Fan, X. Y. Li, Z. Y. Liu, Wang, J. Duan, Moses O. Tadé and S. M. Liu, Facile tailoring of the electronic structure and the d-band center of copper-doped cobaltate for efficient nitrate electrochemical hydrogenation. ACS Appl Mater Interfaces.2022:14:35477-35484.
[10] H. Li, X. Y. Xu, Xi. H. Lin, S. H. Chen, M. Y. He, F. Peng and F. M. Gao, Cooperative interaction between Cu and sulfur vacancies in SnS_2 nanoflowers for highly efficient nitrate electroreduction to ammonia. J. Mater. Chem. A, 2023,11, 2014-2022.
[11] F. C. Lei, K. Li, M. S. Yang, J. Yu, M. M. Xu, Y. M. Zhang, J. F. Xie, P. Hao, G. W. Cui and B. Tang, Electrochemical reduction of nitrate on silver surface and an in-situ Raman spectroscopy study. Inorg. Chem. Front., 2022,9, 2734-2740.